

Proliferation-driven mechanical feedback regulates cell dynamics in growing tissues

Sumit Sinha¹, Xin Li², Abdul N Malmi-Kakkada³, and D. Thirumalai^{1,2}

¹*Department of Physics, University of Texas at Austin, Austin, TX 78712, USA.*

²*Department of Chemistry, University of Texas at Austin, Austin, TX 78712, USA. and*

³*Department of Physics and Biophysics,
Augusta University, Augusta, GA 30912, USA.*

(Dated: May 6, 2024)

Abstract

Local stresses in a tissue, a collective property, regulate cell division and apoptosis. In turn, cell growth and division induce active stresses in the tissue. As a consequence, there is a feedback between cell growth and local stresses. However, how the cell dynamics depend on local stress-dependent cell division and the feedback strength is not fully understood. Here, we probe the consequences of stress-mediated growth and cell division on cell dynamics using agent-based simulations of a two-dimensional growing tissue. We discover a rich dynamical behavior of individual cells, ranging from jamming (mean square displacement, $\Delta(t) \sim t^\alpha$ with α less than unity), to hyperdiffusion ($\alpha > 2$) depending on cell division rate and the strength of the mechanical feedback. Strikingly, $\Delta(t)$ is determined by the tissue growth law, which quantifies cell proliferation (number of cells $N(t)$ as a function of time). The growth law ($N(t) \sim t^\lambda$ at long times) is regulated by the critical pressure that controls the strength of the mechanical feedback and the ratio between cell division-apoptosis rates. We show that $\lambda \sim \alpha$, which implies that higher growth rate leads to a greater degree of cell migration. The variations in cell motility are linked to the emergence of highly persistent forces extending over several cell cycle times. Our predictions are testable using cell-tracking imaging techniques.

I. INTRODUCTION

Cell growth, proliferation, and apoptosis are ubiquitous in biology, and play a crucial role in embryogenesis, tumorigenesis, and wound healing [1, 2]. The breakdown of strict control between cell division and apoptosis rates could lead to fatal diseases like cancer [3]. In cancer metastasis, the cells develop migratory phenotype and invade the surrounding tissues and organs [4]. Therefore, to understand the role of cell division and apoptosis numerous experiments have been performed both in two and three dimensions, which provide the time traces of cells [5–8]. The cell trajectories could be used to calculate dynamical properties of cells [9] that may be quantitatively compared with experiments [10].

An interplay between cell division, apoptosis, and biomechanical feedback determines cell proliferation and the associated dynamics in an evolving tissue. For instance, a growing tissue exhibits a morphological transition, characterized by contrasting collective cell dynamics in the pre-and post-transition phases [5]. Cells in the pre-transition phase exhibit fluid-like behavior whereas those in the post-transition phase are more solid-like [5]. The morphological transition, resulting in the contrasting dynamics, was attributed to the microenvironment-dependent growth and proliferation of cells [5, 11]. The growth of cells in tissue depends on the local stresses, which in turn depend on the local growth rate. In other words, there is a feedback between local stress and cell growth, as was pointed out in a prescient study nearly two decades ago [11]. In addition to fluid and solid-like behavior, the dynamics could also show glassy behavior in confluent [12] and non-confluent tissues [13]. How the mechanical feedback and cell division affects the observed dramatic variations in collective cell dynamics as the tissue grows is largely unknown.

Previous studies that considered cell growth and division on the cell collective dynamics

assumed that the birth rate of cells depends on its coordination number [14]. However, recent experiments report that mere contact between cells may not be sufficient for inhibiting mitosis in cells [5]. Here, using an agent-based model introduced previously [13, 15–18] in which the growth of a cell depends on the local pressure, we establish that the dynamics of cells is linked to the tissue growth law. We show that tissue growth is controlled by two parameters-(a) the critical pressure (p_c) and (b) the birth rate of cells (k_b), which are intrinsic properties of individual cells. The p_c value determines the mechanical feedback strength [19].

The central results of this work are: (a) Depending on the values of p_c and k_b , cells exhibit subdiffusive (the mean-squared displacement, $\Delta(t) \propto t^\alpha, \alpha \leq 1$), superdiffusive ($1 < \alpha \leq 2$) or even hyperdiffusive ($\alpha > 2$) dynamics. On increasing the value of p_c , the cells transition from sub-diffusive to hyperdiffusive dynamics. Surprisingly, on decreasing k_b , the cells switch from sub to super-diffusive or super to hyper-diffusive dynamics. (b) The tissue growth law exhibits a power increase in time (t), $N(t) \propto t^\lambda$, where N is the number of cells. Strikingly, the global growth law is a predictor of the single-cell dynamics. As λ increases, so does α with $\alpha \sim \lambda$. (c) The emergence of persistent forces due to cell division that extends over several cell cycle times is the principal reason for the anomalous (super or hyper-diffusive) cell dynamics. Our work provides a unifying framework for understanding origins of differing dynamical regimes (sub-diffusive [12], diffusive [14] and super-diffusive [13]) in the collective movement of cells driven by mechanical feedback arising from apoptosis and division.

II. METHODS

We briefly explain the off-lattice agent-based computational model used to simulate the spatio-temporal dynamics of a two-dimensional (2D) growing tissue. The computational

model is adopted from previous studies [9, 13, 15–18, 20, 21]. The cells are represented as interacting deformable disks with radius depending on local rules, which assume that cells grow stochastically, and divide upon reaching a critical mitotic size (R_m). The interaction between cells is the sum of elastic and adhesive forces. We also assume that the cells are moving in an overdamped environment in which the inertia is negligible and viscous forces are large compared to environmental fluctuations.

Forces: The elastic (repulsive) force between two disks of radii R_i and R_j is modeled as,

$$F_{ij}^{el}(t) = \frac{h_{ij}^{3/2}(t)}{\frac{3}{4} \left(\frac{1-\nu_i^2}{E_i} + \frac{1-\nu_j^2}{E_j} \right) \sqrt{\frac{1}{R_i(t)} + \frac{1}{R_j(t)}}}, \quad (1)$$

where E_i and ν_i , respectively, are the elastic modulus and Poisson ratio of cell i . The overlap between the disks, if they interpenetrate without deformation, is h_{ij} , which is defined as $\max[0, R_i + R_j - |\vec{r}_i - \vec{r}_j|]$ with $|\vec{r}_i - \vec{r}_j|$ being the center-to-center distance between the two disks.

Cell adhesion, mediated by receptors on the cell surface, enables the cells to stick together. For simplicity, we assume that the receptor and ligand molecules are evenly distributed on the cell surface. Consequently, the magnitude of the attractive adhesive force, F_{ij}^{ad} , between two cells i and j scale as a function of their contact line segment, L_{ij} . Keeping the 3D model as a guide [13], we calculate F_{ij}^{ad} using,

$$F_{ij}^{ad} = L_{ij} f^{ad} \frac{1}{2} (c_i^{rec} c_j^{lig} + c_j^{rec} c_i^{lig}), \quad (2)$$

where the c_i^{rec} (c_i^{lig}) is the receptor (ligand) concentration (assumed to be normalized to the maximum receptor or ligand concentration so that $0 \leq c_i^{rec}, c_i^{lig} \leq 1$). The coupling constant f^{ad} allows us to rescale the adhesion force to account for the variabilities in the maximum densities of the receptor and ligand concentrations. We calculate the contact length, L_{ij} , using the length of contact between two intersecting circles, $L_{ij} = \frac{\sqrt{(|4r_{ij}^2 R_i^2 - (r_{ij}^2 - R_j^2 + R_i^2)|)}}{r_{ij}}$.

Here, r_{ij} is the distance between cells i and j . As before, R_i and R_j denote the radius of cell i and j . In the present case, the strength of repulsive interactions is very large compared to attractive forces which can be seen in Figure 1a.

The the sum of the repulsive and adhesive forces in Eqs.(1) and (2) point along the unit vector \mathbf{n}_{ij} from the center of cell j to the center of cell i . The total force on the i^{th} cell is given by the sum over its nearest neighbors ($NN(i)$),

$$\mathbf{F}_i = \sum_{j \in NN(i)} (F_{ij}^{el} - F_{ij}^{ad}) \mathbf{n}_{ij}. \quad (3)$$

The nearest neighbors satisfy the condition $R_i + R_j - |\mathbf{r}_i - \mathbf{r}_j| > 0$.

Equation of Motion: We used overdamped dynamics of the motion of the i^{th} cell. The equation of motion is,

$$\dot{\mathbf{r}}_i = \frac{\mathbf{F}_i}{\gamma_i}. \quad (4)$$

Here, γ_i is the friction coefficient of the i^{th} cell. We assume γ_i to be equal to $cR_i(t)$, where c is a constant. Note, we neglect temperature effects because the drag forces are high [14] compared to environmental fluctuations.

Cell growth, division, and apoptosis: In the model, cells are either dormant (D) or in the growth (G) phase depending on the magnitude of the local pressure of the cell (see Figure 1b for a schematic). Using Irving-Kirkwood's definition, we calculate the pressure (p_i) on the i^{th} cell due to contact with its neighbors [22] using,

$$p_i = \frac{1}{2} \sum_{j \in NN(i)} \frac{\mathbf{F}_{ij} \cdot \mathbf{dr}_{ij}}{A_i}, \quad (5)$$

where A_i is local area of influence, equal to $\theta\pi R_i^2$. We used $\theta = 1.5$, in our simulations. If the local pressure on the i^{th} cell, p_i , exceeds a critical value (p_c) the cell ceases to grow and enters the dormant phase. Note that the cell can switch to the growth phase if $\frac{p_i}{p_c} < 1$ at a later time. The critical pressure, p_c , serves as a mechanical feedback [11]. The local

pressure, p_i , can easily exceed p_c if it is small. In this case, most cells would be dormant for a long time. In the opposite limit, $p_c \gg p_i$, it is unlikely that the cells would reach the dormant phase. This would result in cell proliferation. Thus, p_c is the strength of the mechanical feedback. A previous study used p_c to control cell growth in confined spaces in a different context [19]. It was shown there is a growth-driven jamming transition, controlled by the strength ($\propto \frac{1}{p_c}$) of the mechanical feedback. They did not consider cell dynamics, which is the focus of our investigation.

For growing cells, we assume that the area increases at a constant rate r_A as the cell cycle progresses. The cell radius is updated from a Gaussian distribution with the mean rate $\dot{R} = (2\pi R)^{-1}r_A$. Over the cell cycle time τ , r_A is taken to be,

$$r_A = \frac{\pi(R_m)^2}{2\tau}, \quad (6)$$

where R_m is the mitotic radius. The cell cycle time is related to the growth rate (k_b) by $\tau = \frac{\ln 2}{k_b}$. A cell divides once it grows to the fixed mitotic radius (R_m). To ensure the total area of a cell is conserved upon cell division, we use $R_d = R_m 2^{-1/2}$ as the radius of the daughter cells. The mother and daughter cells are placed at a center-to-center distance, $d = 2R_m(1 - 2^{-1/2})$ upon cell division. The direction of the new cell location is chosen randomly from a uniform distribution on the unit circle. One source of stochasticity in the cell movement is the random choice for the mitotic direction. The cells can also undergo apoptosis at rate k_a . In all the simulations, we vary k_b but the apoptosis rate (k_a) is fixed to $10^{-6} s^{-1}$. The values of the parameters used in the simulations are given in Table 1.

We initiated the simulations by placing 100 cells on a 2D plane whose coordinates are chosen from a normal distribution with zero mean, and standard deviation $25 \mu m$. All the parameters except p_c and k_b are fixed. All the simulations are terminated when the scaled time $t^* = (k_b - k_a)t \sim 3.74$. A representative snapshot of the growing tissue is shown in

Figure 1c.

Table I: The parameters used in the simulations.

Parameters	Values	References
Timestep (Δt)	10s	This paper
Critical Radius for Division (R_m)	5 μm	[13, 16]
Friction coefficient ($\frac{\gamma_i}{R_i}$)	0.0942 kg/($\mu\text{m s}$)	This paper
Cell Cycle Time (τ_{min})	54000 s	[13, 23–25]
Adhesive Coefficient (f^{ad})	$10^{-4} \mu\text{N}/\mu\text{m}$	This paper
Mean Cell Elastic Modulus (E_i)	10^{-3}MPa	[13, 26]
Mean Cell Poisson Ratio (ν_i)	0.5	[13, 16]
Death Rate (k_a)	10^{-6}s^{-1}	[13]
Mean Receptor Concentration (c^{rec})	1.0 (Normalized)	[13]
Mean Ligand Concentration (c^{lig})	1.0 (Normalized)	[13]

III. RESULTS

A. Increasing p_c with $\frac{k_b}{k_a}$ fixed enhances cell motility

Local stress regulates cell division propensity, and hence, should influence the cell dynamics in a growing tissue. To assess the effect of feedback on cell dynamics, we varied p_c , strength of the feedback. The dynamics are probed using the mean squared displacement ($\Delta(t)$),

$$\Delta(t) = \frac{1}{N} \sum_{i=0}^{i=N} [\mathbf{r}_i(t) - \mathbf{r}_i(0)]^2, \quad (7)$$

where $\mathbf{r}_i(t)$ is the position of the i^{th} cell at time t , and N is the number of cells. We also calculated the tissue boundary, $\Delta r(t)$, an estimate of the tissue size, using,

$$\Delta r(t) = \frac{1}{N_b(t)} \sum_{i=1}^{N_b} |\mathbf{r}_i(t) - \mathbf{R}(t)| \quad (8)$$

where $N_b(t)$ is the total number of boundary cells at time t and $\mathbf{R}(t)$ is the center of the tumor at time t . These quantities can be readily measured using imaging experiments [5, 6].

Figure 2a shows the time dependence of $\Delta(t)$ for three values of p_c : $10^{-5}Nm^{-1}$, $10^{-4}Nm^{-1}$ and $10^{-3}Nm^{-1}$ for a fixed $\frac{k_b}{k_a} = 20$. Because the cells undergo apoptosis, we included only the cells that were present throughout the simulations in calculating $\Delta(t)$. In the intermediate time limit, $t < \frac{1}{k_b - k_a}$, the dynamics is subdiffusive ($\Delta(t) \sim t^\delta, \delta < 1$) for the three p_c values. The long time ($t > \frac{1}{k_b - k_a}$) dynamics depends on the p_c . We find that $\Delta(t) \sim (t^*)^\alpha$ is subdiffusive ($\alpha = 0.68$) for $p_c = 10^{-5}Nm^{-1}$, superdiffusive ($\alpha = 1.36$) for $p_c = 10^{-4}Nm^{-1}$ and hyperdiffusive ($\alpha = 3$) for $p_c = 10^{-3}Nm^{-1}$. As the mechanical feedback strength increases, which is realized by decreasing p_c , the cells are jammed, resulting in slow dynamics at small p_c . Increased cell proliferation with weaker mechanical feedback (larger p_c) gives rise to superdiffusive or even hyperdiffusive dynamics.

The invasion distance increases algebraically with time, $\Delta r(t) \sim (t^*)^\xi$, (the time $t^* = (k_b - k_a)t$) where ξ characterizes the tissue invasion propensity. Figure 2b shows $\Delta r(t)$ for p_c equal to $10^{-5}Nm^{-1}$, $10^{-4}Nm^{-1}$ and $10^{-3}Nm^{-1}$ with $\frac{k_b}{k_a} = 20$. We find (Figure 2b) that the growing tissue is maximally invasive for $p_c = 10^{-3}Nm^{-1}$ similar to behavior of $\Delta(t)$. For $p_c = 10^{-5}Nm^{-1}$, $\xi = 0.34$, for $p_c = 10^{-4}Nm^{-1}$, $\xi = 0.68$ and for $p_c = 10^{-3}Nm^{-1}$, $\xi = 1.23$. We surmise from the behavior of $\Delta(t)$ and $\Delta r(t)$ that the tissue dynamics is enhanced upon increasing p_c at a fixed value of $\frac{k_b}{k_a}$. This is because the probability that the cells are in the growth phase increases as p_c increases.

B. Decreasing $\frac{k_b}{k_a}$ with p_c fixed promotes cell migration

We next varied the cell division rate (k_b) at a fixed $k_a = 10^{-6}s^{-1}$. Figure 2c shows $\Delta(t)$ as a function of t for $\frac{k_b}{k_a} = 20, 8$ and 2 at a fixed $p_c = 10^{-4}Nm^{-1}$. Surprisingly, in the long time ($[k_b - k_a]t > 1$) limit, slower dividing cells have higher motility. For instance, $\frac{k_b}{k_a} = 20$, the MSD exponent values ($\Delta(t) \sim (t^*)^\alpha$ at long times), are $\alpha = 1.36$, for $\frac{k_b}{k_a}$ equal to 8 , $\alpha = 1.67$ and for $\frac{k_b}{k_a}$ equal to 2 , $\alpha = 2.90$. We observed similar behavior for $\Delta r(t)$ on decreasing $\frac{k_b}{k_a}$. As before, we expressed $\Delta r(t) \sim (t^*)^\xi$. For $\frac{k_b}{k_a}$ equal to 20 , $\xi = 0.68$, for $\frac{k_b}{k_a}$ equal to 8 , $\xi = 0.85$ and for $\frac{k_b}{k_a}$ equal to 2 , $\xi = 1.23$.

The time dependent changes in $\Delta r(t)$ and $\Delta(t)$ shows that the degree of migration, quantified using ξ and $\bar{\alpha}$, is enhanced upon decreasing $\frac{k_b}{k_a}$ as long as p_c is fixed.

C. Growth law dictates the dynamics of cells

What is the unifying explanation for the non-trivial cell dynamics in an evolving cell colony as p_c and k_b are varied? The answer lies in the growth law of the tissue. The experimental growth law is determined by counting the number of cells as a function of time [5]. The growth law is an emergent property that depends not only on the properties of individual cells but also the coupling, through the mechanical feedback and adhesive interactions.

Changing p_c : We first calculated the number of cells (N) as a function of time at $p_c = 10^{-5}Nm^{-1}, 10^{-4}Nm^{-1}$ and $10^{-3}Nm^{-1}$ with $\frac{k_b}{k_a} = 20$ (Figure 3a). We find that $N(t)$ increases as, $N(t) \sim t^\lambda$. For $p_c = 10^{-5}Nm^{-1}$, $\lambda = 1$, for $p_c = 10^{-4}Nm^{-1}$, $\lambda = 1.31$ and for $p_c = 10^{-3}Nm^{-1}$, $\lambda = 2.78$. It is clear that growth rate increases as the mechanical feedback strength decreases (Figure 3a). To determine the origin of the enhanced growth at as p_c

increases, we calculated the average pressure, $\langle p(t) \rangle = \frac{1}{N} \sum_{i=1}^N p_i$ (Figure 3b). For $p_c = 10^{-5}$, the average value of $\langle p(t) \rangle$ is higher than the critical pressure, which implies that the cells are predominantly in the dormant phase. For $p_c = 10^{-4}$, $\langle p(t) \rangle$ exceeds p_c after a few cell cycle times, and thus the cells start entering dormancy. However, for $p_c = 10^{-3}$, $\langle p(t) \rangle$ is always smaller than p_c , which implies the majority of the cells are in the growth phase, resulting in increased cell division, and proliferation.

Changing $\frac{k_b}{k_a}$: We then calculated $N(t)$ at the fixed value of $p_c = 10^{-4}$ for three values of $\frac{k_b}{k_a} = 20, 8$ and 2 . Figure 3c shows $N(t)$ as a function of $\frac{k_b}{k_a}$. The growth exponents ($N(t) \sim t^\lambda$) are $\lambda = 1.31$, $\lambda = 1.69$ and $\lambda = 2.60$ for $\frac{k_b}{k_a} = 20$, $\frac{k_b}{k_a} = 8$, $\frac{k_b}{k_a} = 2$, respectively. Strikingly, tissue growth rate decreases as cell division rate increases, which may be understood in terms of the dynamic changes in the average pressure, $\langle p(t) \rangle$, plotted in Figure 3d, as a function of $\frac{k_b}{k_a}$. Upon decreasing $\frac{k_b}{k_a}$, the generation of pressure in the tissue is suppressed. For $\frac{k_b}{k_a} = 2$, the $\langle p(t) \rangle$ is smaller than p_c for long times (exceeding the cell division time) unlike the case for $\frac{k_b}{k_a} = 20$ and 8 . Therefore, multiples cell divisions occur in cells that divide slowly compared to those that divide fast, thus resulting in greater tissue growth. Our analyses show that for both conditions (changing p_c and $\frac{k_b}{k_a}$), the growth law of the tissue determines the cell dynamics.

D. Emergence of highly correlated force

To gain mechanistic understanding of the emergent anomalous dynamics of individual cells, we calculated the force autocorrelation function, $\text{FAF}(t^*) = \frac{\langle \mathbf{F}(t+t^*) \cdot \mathbf{F}(t) \rangle_t}{\langle \mathbf{F}(t) \cdot \mathbf{F}(t) \rangle_t}$ [20]. In an overdamped system, the FAF encodes the directed nature of motion in individual cells. Here, $\mathbf{F}(t)$ is the force on the cell at time t and $\langle \dots \rangle_t$ is the time average. Figure 4 shows the plot of FAF for a fixed $\frac{k_b}{k_a} = 20$ for $p_c = 10^{-3} Nm^{-1}$, $10^{-4} Nm^{-1}$ and $10^{-5} Nm^{-1}$. It shows that

the FAF decays via a two steps, characterized by short ($\frac{\gamma}{ER_m}$) and long ($\sim \frac{1}{k_b - k_a}$) times. To extract the two-time scales, we fit FAF using $Ae^{-\frac{t}{\tau_c}} + C$ in both the regimes.

At short times (see the inset of Figure 4), for $p_c = 10^{-3}Nm^{-1}$, $A = 0.5$, $\tau_c = \frac{1.2\gamma}{ER_m}$ and $C = 0.42$. For $p_c = 10^{-4}Nm^{-1}$, $A = 0.75$, $\tau_c = \frac{0.97\gamma}{ER_m}$ and $C = -0.02$. Lastly, for $p_c = 10^{-5}Nm^{-1}$, $A = 0.81$, $\tau_c = \frac{0.95\gamma}{ER_m}$ and $C = 0.1$. It is clear that at short times, the relaxation time is approximately close to the elastic time scale $\frac{\gamma}{ER_m}$, which is negligible compared to $\frac{1}{k_b - k_a}$.

In the long time limit, the FAF exhibits correlations. For $p_c = 10^{-3}Nm^{-1}$, $A = 0.4$, $\tau_c = \frac{2.2}{k_b - k_a}$ and $C = -0.06$. For $p_c = 10^{-4}$, $A = 0.12$, $\tau_c = \frac{2.3}{k_b - k_a}$ and $C = -0.02$. Lastly, for $p_c = 10^{-5}Nm^{-1}$, $A = 0.04$, $\tau_c = \frac{0.2}{k_b - k_a}$ and $C = 0.003$. For $p_c = 10^{-5}Nm^{-1}$, A is negligible, implying the absence of correlations force, which explains the observed subdiffusive dynamics. The value of A for $p_c = 10^{-3}Nm^{-1}$ is four times larger than for $p_c = 10^{-4}Nm^{-1}$. In addition, the FAF decays over (2-3) cell division times when the feedback strength is high. Larger magnitude of FAF in the long time regime leads to higher degree of migration for $p_c = 10^{-3}Nm^{-1}$.

E. Diagram of states

The simulation results in Figure 3 suggest that the cell dynamics is determined by the tissue growth law. The generality of this result follows from the following arguments. If the overall shape of the tissue is circular in 2D (see Figure 1c), we expect the exponents α ($\Delta(t) \sim t^\alpha$) and λ ($N(t) \sim t^\lambda$) should have similar values with $\alpha \approx \lambda$. From the algebraic growth of the tissue, it follows that $N(t) \sim t^\lambda \sim r^2$, which holds for a circular shape. From the relation $r^2 \sim \Delta(t) \sim t^\alpha$, expect that $\alpha \sim \lambda$. In addition, the exponents ξ ($\Delta r(t) \sim t^\xi$) and λ should be related as $\lambda \approx 2\xi$. The results in Figures 5a show that the relation is

approximately satisfied.

Based on the findings in Figures 5a we are able to predict a diagram of states as a function of p_c and $\frac{k_b}{k_a}$. Recent works probing the effect of cell division and apoptosis have reported subdiffusive [12], diffusive [14], and superdiffusive motion [13]. However, the regime in which these values emerge is unclear. Furthermore, time traces of cell positions maybe be recorded using particle tracking techniques. In anticipation of such experiments, we characterized single-cell dynamics by calculating the mean squared displacement over a broad range of p_c and $\frac{k_b}{k_a}$. We extracted the α exponent in the long time limit. The value of α could be used to determine the nature of dynamics in the time regime of interest. Figure 5b shows the two-dimensional diagram of states. Interestingly, we observe all three regimes of motion, subdiffusive, superdiffusive, and hyperdiffusive, by varying $\frac{k_b}{k_a}$ and p_c .

Figure 5b reveals three interesting characteristics of cell dynamics driven by cell division and apoptosis: (a) Upon increasing p_c , there is a transition from subdiffusive to superdiffusive, and finally hyperdiffusive diffusive behavior. At a fixed $\frac{k_b}{k_a} = 20$, for $p_c = 5 \times 10^{-6} Nm^{-1}$ dynamics is subdiffusive, for $p_c = 10^{-4} Nm^{-1}$ cells exhibit superdiffusive motion. Upon further increasing p_c to $10^{-3} Nm^{-1}$, hyperdiffusive dynamics is observed. (b) Surprisingly, upon decreasing $\frac{k_b}{k_a}$, α increases. For smaller (higher) p_c values, on decreasing $\frac{k_b}{k_a}$, the dynamics change from subdiffusive (superdiffusive) to superdiffusive (hyperdiffusive) behavior. For fixed $p_c = 10^{-5} Nm^{-1}$, at $\frac{k_b}{k_a} = 20$ ($\frac{k_b}{k_a} = 2$), we observe subdiffusion (superdiffusion). For a higher value of $p_c = 10^{-4} Nm^{-1}$, at $\frac{k_b}{k_a} = 20$ ($\frac{k_b}{k_a} = 2$), the dynamics is superdiffusive ion (hyperdiffusive). The diagram of states (Figure 5b) was created using a smoothing procedure where the values of the MSD exponents at unknown values of $\frac{k_b}{k_a}$ and p_c were interpolated using the known MSD values (obtained via simulations). The interpolation is logarithmically (linearly) scaled in p_c ($\frac{k_b}{k_a}$) axis. The two-dimensional phase diagram predicts the emergence

of different dynamical regimes, from subdiffusive to hyperdiffusive, which can be tested in imaging experiments [5, 6].

IV. CONCLUSION

Using a two-dimensional off-lattice model, we have provided a comprehensive picture of the variations in the dynamics as the strength of the mechanical feedback and cell division rates are altered. The dynamics change from subdiffusive to superdiffusive to hyperdiffusive, as the $\frac{k_b}{k_a}$ and p_c are varied. We also showed that in growing tissue, highly persistent forces emerge as the strength of the mechanical feedback increases, whose decay exhibits two relaxation time scales: one short (elastic time scale, $\frac{\gamma}{ER_m}$) and one long (division-apoptosis time scale, $\frac{1}{k_b - k_a}$). The presence of persistent forces determines variations in the dynamics as cell division rates and the strength of the feedback are varied. Strikingly, the cell dynamics are controlled by the growth law of the tissue, which depends primarily on the strength of the mechanical feedback. Interestingly, the three exponents α , λ and ξ from cell dynamics and tissue growth are related as $\alpha \approx \lambda \approx 2\xi$. Therefore, we can estimate the values of the other two exponents if one of them is obtained in experiments. The phase diagram summarizing our findings provides a unified picture of the disparate dynamics found in several theoretical studies. [12–14]

Acknowledgements: This work was supported by a grant from the National Science Foundation (Phy 23-10639) and the Welch Foundation (F-0019).

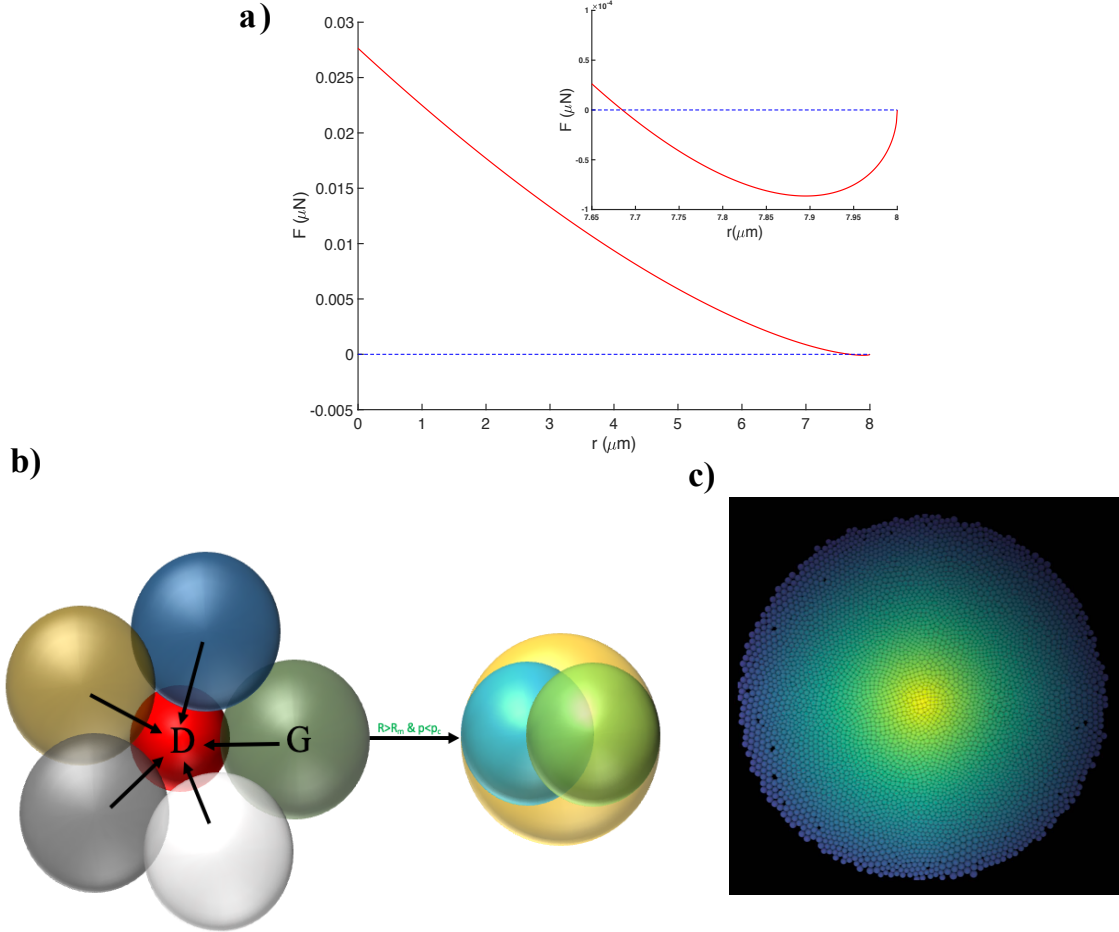


Figure 1: The 2D model. (a) Inter-cellular force as a function of distance between two cells with identical radii, $R_i = R_j = 4\mu m$. The repulsive and attractive parts of the force are given by Eqs. (1) and (2), respectively. The inset is the zoomed-in view that highlights the region in which the force is predominantly attractive. (b) Illustration of the role of mechanical feedback. On the left, the “red” cell is dormant (cannot grow and divide) because the pressure exerted by the neighbors exceeds p_c . The “green” cell is in the growth phase (G) ($p < p_c$). The green cell from the left gives birth to two daughter cells (cyan and green) when the radius exceeds the mitotic radius R_m . (c) A snapshot of the 2D growing tissue consisting of approximately 4,750 cells at $t^* = 3.74$, with $p_c = 10^{-3} MPa$ and $\frac{k_b}{k_a} = 20$. The global shape is approximately circular.

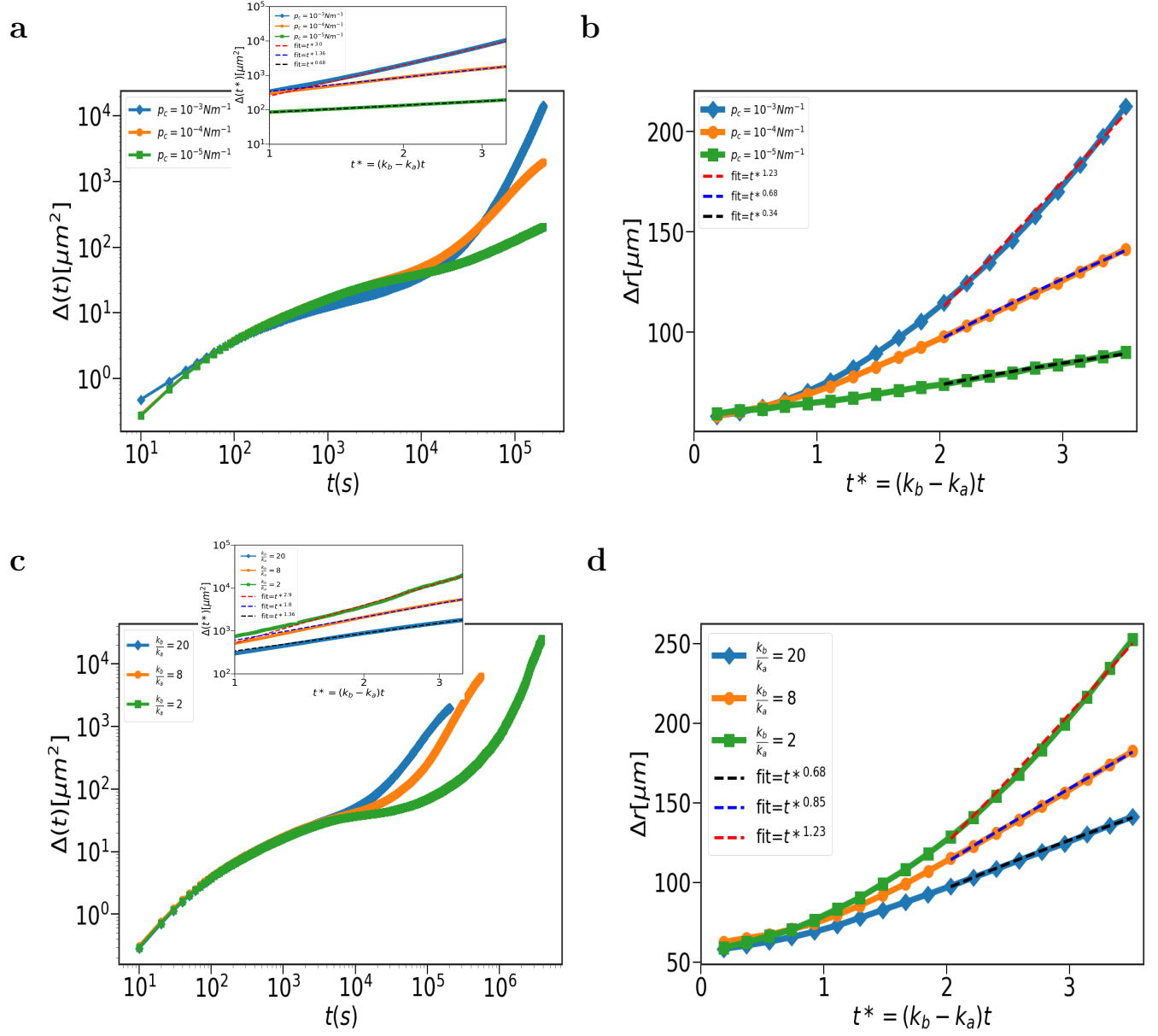


Figure 2: Cell dynamics is regulated by p_c and $\frac{k_b}{k_a}$: (a) Mean squared displacement, $\Delta(t)$, as a function of time. From top to bottom, the curves are for $p_c = 10^{-3} \text{ Nm}^{-1}, 10^{-4} \text{ Nm}^{-1}$ and 10^{-5} Nm^{-1} . The inset focuses on the long time limit ($t > \frac{1}{k_b - k_a}$). The x-axis is scaled by $k_b - k_a$. The dashed lines are power law fits ($\Delta(t) \sim t^\alpha$). The α values are given in the upper left box. (Continued on the next page)

Figure 2: **(b)** Invasion distance, $\Delta r(t)$ as a function of time for different p_c values. The dashed lines are power-law fits ($\Delta r \sim (t^*)^\xi$). The ξ values are given in the upper left box. **(c)** $\Delta(t)$, as a function of time. From left to right, curves correspond to $\frac{k_b}{k_a} = 20, 8$ and 2 . The inset focuses on the long time regime ($t > \frac{1}{k_b - k_a}$). The dashed lines are the power law fits ($\Delta(t) \sim (t^*)^\alpha$). The α values are given in the upper left box. **(d)** Invasion distance, $\Delta r(t)$ as a function of time for changing $\frac{k_b}{k_a}$. The dashed line is the power law fit ($\Delta r \sim (t^*)^\xi$). The ξ values are given in the upper left box.

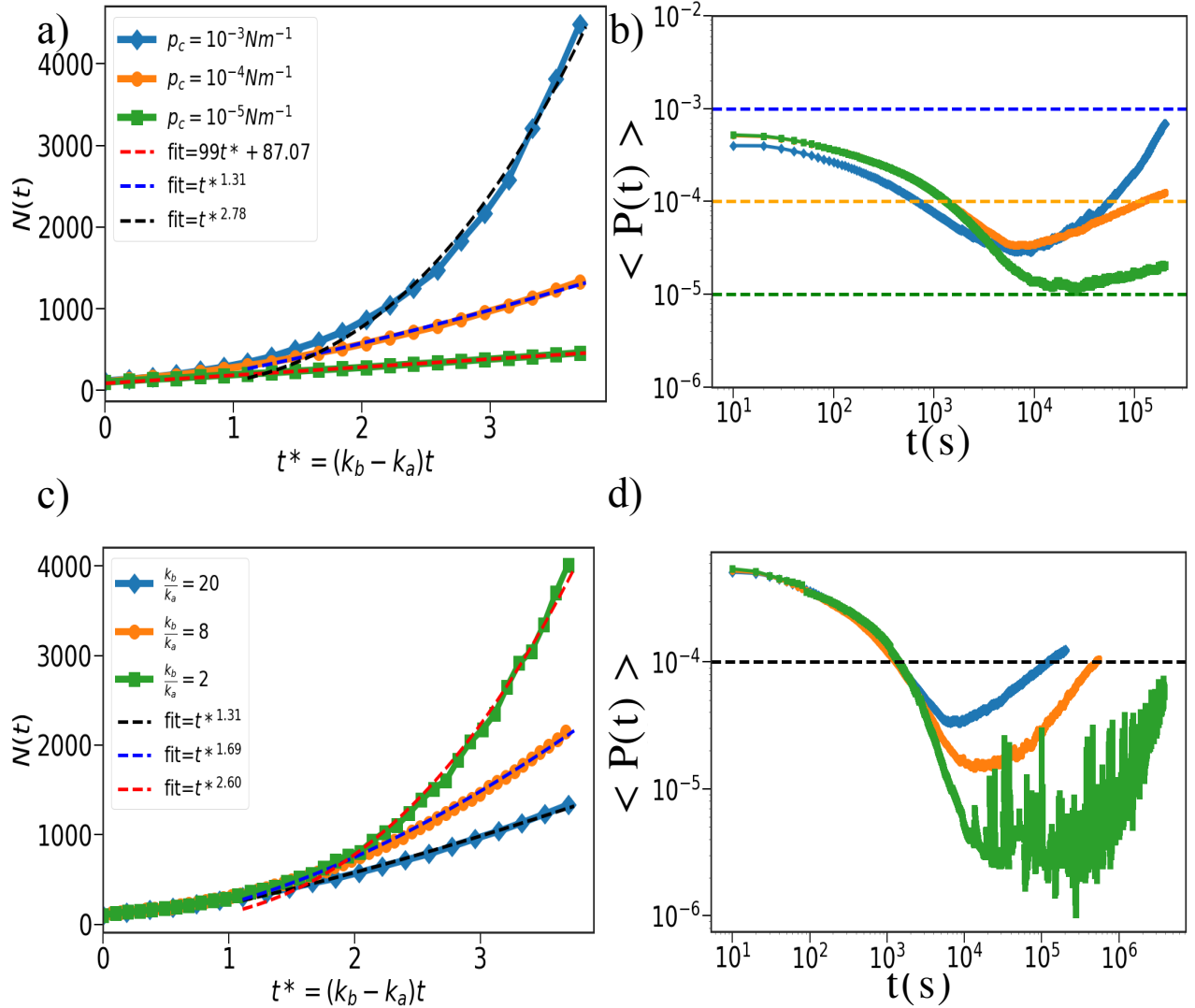


Figure 3: Growth law governs the cell dynamics: (a) Number of cells, $(N(t))$, as a function of time at three values of p_c , labeled in the figure. The dashed lines with the power the power law fits ($N(t) \sim (t^*)^\lambda$) are shown. (b) Average pressure, $\langle P(t) \rangle$, as a function of time. The curves correspond to $p_c = 10^{-3} Nm^{-1}$ (top), $10^{-4} Nm^{-1}$ (middle), and $10^{-5} Nm^{-1}$ (bottom). The dashed lines mark the p_c values; blue - $p_c = 10^{-3} Nm^{-1}$, orange - $p_c = 10^{-4} Nm^{-1}$, and green - $p_c = 10^{-5} Nm^{-1}$. (Continued on the next page).

Figure 3: (c) $N(t)$, as a function of time. From bottom to top, curves correspond to $\frac{k_b}{k_a} = 20$ (blue), 8 (orange) and 2 (green). The dashed lines are the power law fits. The λ values are mentioned in the upper left box. (d) Average pressure, $\langle P(t) \rangle$, as a function of time for the three $\frac{k_b}{k_a}$ values. From bottom to top, curves correspond to $\frac{k_b}{k_a} = 20$ (blue), 8 (orange) and 2 (green). The dashed line corresponds to a pressure equal to $10^{-4} Nm^{-1}$.

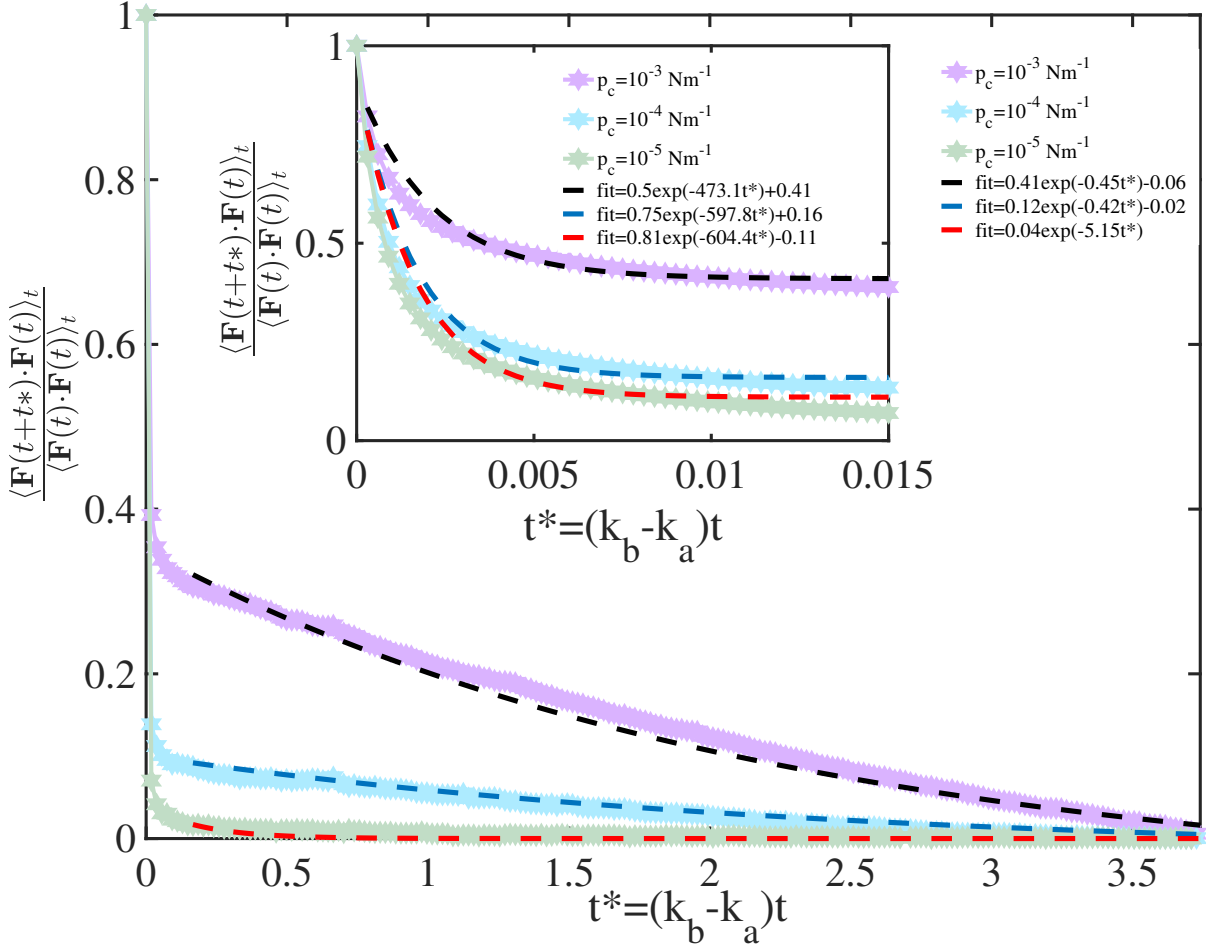


Figure 4: Correlation in force: Force autocorrelation function (FAF) as a function of time. From top to bottom, FAF corresponds to $p_c = 10^{-3}, 10^{-4}$ and 10^{-5} . The dashed lines are the fits. Inset is the zoomed of the initial times. The figure shows the emergence of FAF with two-time scales: long ($\sim \frac{1}{k_b - k_a}$) and short (elastic time scale = $\frac{\gamma}{ER}$).

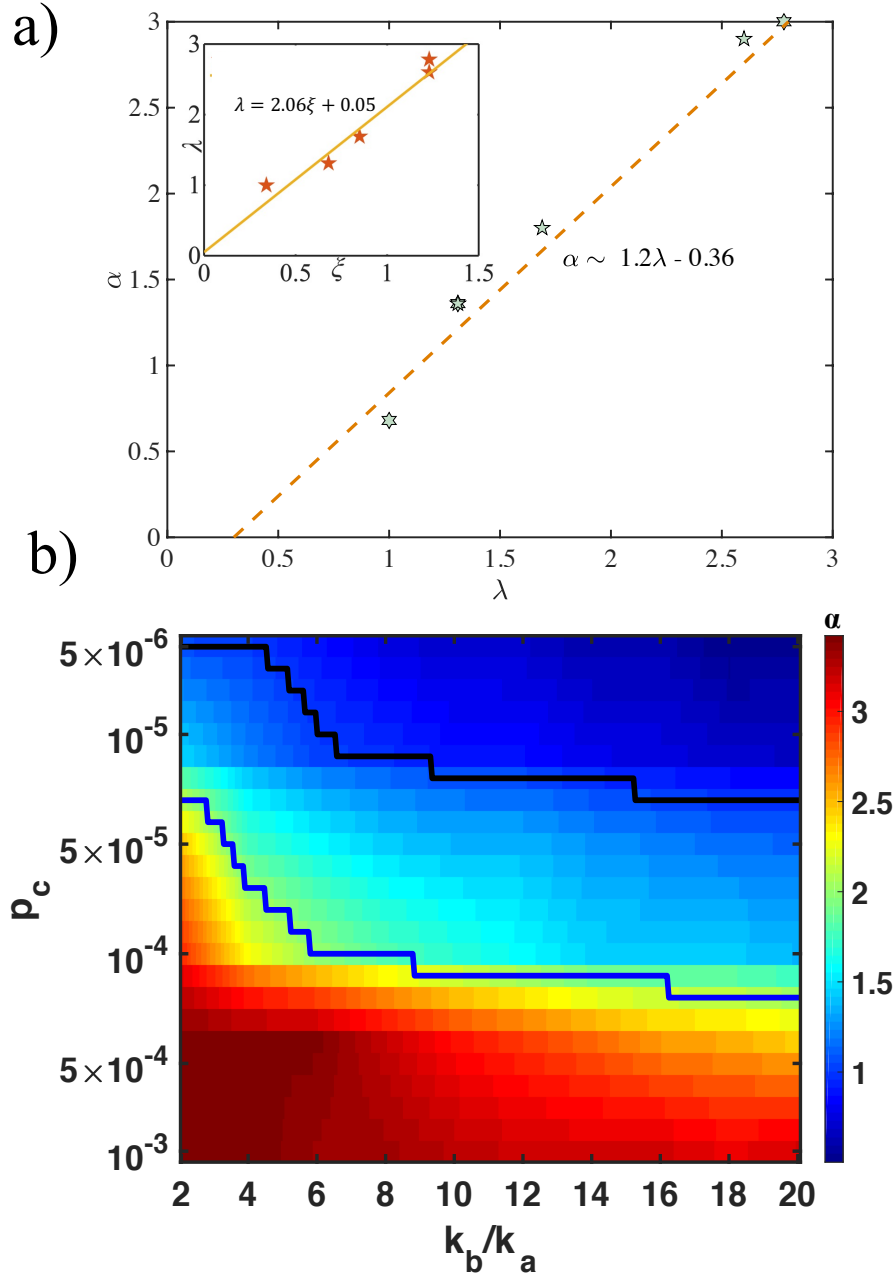


Figure 5: Dynamical phase diagram : (a) The MSD exponent α as a function of the growth law exponent λ . The slope of the dashed line is approximately unity. In the inset we plot the relationship between λ and ξ . The fit of the line is $\lambda \approx 2\xi$. (b) Dynamical regimes as a phase diagram in the plane of p_c and $\frac{k_b}{k_a}$. The color bar on the right shows the value of α . Sub-diffusion ($\alpha \leq 1$), superdiffusion ($1 < \alpha \leq 2$), and hyper-diffusion ($\alpha > 2$) in the long-time cell dynamics ($(k_b - k_a)t > 1$). The black (blue) lines correspond to $\alpha = 1$ ($\alpha = 2$).

Figure 5: The two-dimensional phase diagram predicts the emergence of subdiffusion, superdiffusion, and hyperdiffusion, depending on the values of p_c and $\frac{k_b}{k_a}$. The phase diagram was obtained via a smoothing procedure (details in the text)

-
- [1] BA Barres, IK Hart, HSR Coles, JF Burne, JT Voyvodic, WD Richardson, and MC 1992 Raff. Cell death and control of cell survival in the oligodendrocyte lineage. *Cell*, 70(1):31–46, 1992.
- [2] Thomas Lecuit and Loïc Le Goff. Orchestrating size and shape during morphogenesis. *Nature*, 450(7167):189, 2007.
- [3] Robert A Weinberg. *The Biology of Cancer: Second International Student Edition*. WW Norton & Company, 2013.
- [4] Sanjay Kumar and Valerie M Weaver. Mechanics, malignancy, and metastasis: the force journey of a tumor cell. *Cancer and Metastasis Reviews*, 28(1-2):113–127, 2009.
- [5] Alberto Puliafito, Lars Hufnagel, Pierre Neveu, Sebastian Streichan, Alex Sigal, D Kuchnir Fygenon, and Boris I Shraiman. Collective and single cell behavior in epithelial contact inhibition. *Proceedings of the National Academy of Sciences*, 109(3):739–744, 2012.
- [6] Angela M Jimenez Valencia, Pei-Hsun Wu, Osman N Yogurtcu, Pranay Rao, Josh DiGiacomo, Inês Godet, Lijuan He, Meng-Horng Lee, Daniele Gilkes, Sean X Sun, et al. Collective cancer cell invasion induced by coordinated contractile stresses. *Oncotarget*, 6(41):43438, 2015.
- [7] Yu Long Han, Adrian F Pegoraro, Hui Li, Kaifu Li, Yuan Yuan, Guoqiang Xu, Zichen Gu, Jiawei Sun, Yukun Hao, Satish Kumar Gupta, et al. Cell swelling, softening and invasion in a three-dimensional breast cancer model. *Nature physics*, 16(1):101–108, 2020.
- [8] Jae Hun Kim, Adrian F Pegoraro, Amit Das, Stephan A Koehler, Sylvia Ann Ujwary, Bo Lan, Jennifer A Mitchel, Lior Atia, Shijie He, Karin Wang, et al. Unjamming and collective migration in mcf10a breast cancer cell lines. *Biochemical and biophysical research communications*,

- 521(3):706–715, 2020.
- [9] Sumit Sinha and D Thirumalai. Self-generated persistent random forces drive phase separation in growing tumors. *The Journal of Chemical Physics*, 153(20), 2020.
- [10] A. M. J. Valencia, P.-H. Wu, O. N. Yogurtcu, P. Rao, J. DiGiacomo, I. Godet, L. He, M.-H. Lee, D. Gilkes, S. X. Sun, and D. Wirtz. *Oncotarget*, 6:43438, 2015.
- [11] Boris I Shraiman. Mechanical feedback as a possible regulator of tissue growth. *Proceedings of the National Academy of Sciences*, 102(9):3318–3323, 2005.
- [12] Michael Czajkowski, Daniel M Sussman, M Cristina Marchetti, and M Lisa Manning. Glassy dynamics in models of confluent tissue with mitosis and apoptosis. *Soft matter*, 15(44):9133–9149, 2019.
- [13] Abdul N Malmi-Kakkada, Xin Li, Himadri S Samanta, Sumit Sinha, and Dave Thirumalai. Cell growth rate dictates the onset of glass to fluidlike transition and long time superdiffusion in an evolving cell colony. *Physical Review X*, 8(2):021025, 2018.
- [14] DA Matoz-Fernandez, Kirsten Martens, Rastko Sknepnek, JL Barrat, and Silke Henkes. Cell division and death inhibit glassy behaviour of confluent tissues. *Soft matter*, 13(17):3205–3212, 2017.
- [15] Dirk Drasdo and Stefan Höhme. A single-cell-based model of tumor growth in vitro: monolayers and spheroids. *Physical biology*, 2(3):133, 2005.
- [16] Gernot Schaller and Michael Meyer-Hermann. Multicellular tumor spheroid in an off-lattice voronoi-delaunay cell model. *Physical Review E*, 71(5):051910, 2005.
- [17] Abdul N Malmi-Kakkada, Sumit Sinha, Xin Li, and D Thirumalai. Adhesion strength between cells regulate nonmonotonic growth by a biomechanical feedback mechanism. *Biophysical Journal*, 121(19):3719–3729, 2022.

- [18] Sumit Sinha, Abdul N Malmi-Kakkada, Xin Li, Himadri S Samanta, and D Thirumalai. Spatially heterogeneous dynamics of cells in a growing tumor spheroid: Comparison between theory and experiments. *Soft matter*, 16(22):5294–5304, 2020.
- [19] Pawel Gniewek, Carl F Schreck, and Oskar Hallatschek. Biomechanical feedback strengthens jammed cellular packings. *Physical review letters*, 122(20):208102, 2019.
- [20] Sumit Sinha, Xin Li, Rajsekhar Das, and D Thirumalai. Mechanical feedback controls the emergence of dynamical memory in growing tissue monolayers. *The Journal of Chemical Physics*, 156(24), 2022.
- [21] Bryan A Nerger, Sumit Sinha, Nathan N Lee, Maria Cheriyan, Pascal Bertsch, Christopher P Johnson, L Mahadevan, Joseph V Bonventre, and David J Mooney. 3d hydrogel encapsulation regulates nephrogenesis in kidney organoids. *Advanced Materials*, page 2308325.
- [22] Xingbo Yang, M Lisa Manning, and M Cristina Marchetti. Aggregation and segregation of confined active particles. *Soft matter*, 10(34):6477–6484, 2014.
- [23] James P Freyer and Robert M Sutherland. Regulation of growth saturation and development of necrosis in emt6/ro multicellular spheroids by the glucose and oxygen supply. *Cancer research*, 46(7):3504–3512, 1986.
- [24] Joseph J Casciari, Stratis V Sotirchos, and Robert M Sutherland. Variations in tumor cell growth rates and metabolism with oxygen concentration, glucose concentration, and extracellular ph. *Journal of cellular physiology*, 151(2):386–394, 1992.
- [25] Jacques Landry, James P Freyer, and Robert M Sutherland. Shedding of mitotic cells from the surface of multicell spheroids during growth. *Journal of cellular physiology*, 106(1):23–32, 1981.
- [26] Jörg Galle, Markus Loeffler, and Dirk Drasdo. Modeling the effect of deregulated proliferation

and apoptosis on the growth dynamics of epithelial cell populations in vitro. *Biophysical journal*, 88(1):62–75, 2005.